Imaging ^{55}Fe Electron Tracks in a GEM-based TPC Using a CCD Readout

N. S. Phan[a,*], E. R. Lee[a], D. Loomba[a]

[a]*Department of Physics and Astronomy, University of New Mexico, NM 87131, USA*

arXiv:1703.09883v1 [physics.ins-det] 29 Mar 2017

Abstract

The first optically resolved electron tracks from an ^{55}Fe X-ray source are presented together with the resulting energy spectrum. These tracks were produced in a TPC operating in low pressure carbon tetrafluoride (CF_4) gas, and imaged using a fast lens and low noise CCD optical system. Using GEM/THGEM amplification devices, effective gas gains of $\gtrsim 2\times10^5$ were obtained in pure CF_4 at low pressures in the 25-100 Torr range. The detector's very high signal-to-noise and the low gas pressures allowed individual ionization tracks from 5.9 keV X-ray interactions to be imaged and resolved. The ability to resolve tracks of such low energies has important applications in dark matter and other rare event searches, as well as in X-ray polarimetry. A practical application of the optical signal from ^{55}Fe is that it provides a tool for mapping the detector spatial uniformity.

Keywords: Optical TPC, ^{55}Fe electron tracks, GEMs, Thick GEMs, CF_4, CCD camera

1. Introduction

The capability of a high resolution and high signal-to-noise detector used to study properties of low energy recoils is demonstrated. Motivated by directional searches for dark matter, all measurements were taken at low pressures in the 25-100 Torr range, where low energy tracks are long enough to be resolved. We show that at these low pressures, with sufficient gas gain and light collection efficiency, the electron tracks produced from interactions of 5.9 keV ^{55}Fe X-rays can be *optically* imaged and resolved using a low-noise, high quantum efficiency CCD (charge-coupled device) camera. Optical ^{55}Fe spectra have been obtained with a PMT readout for a GEM-based detector in 750 Torr He/CF_4[1] and a capillary plate detector in 760 Torr Ar/CF_4 [2, 3] but, to our knowledge, this is the first time it has been done using a CCD imaging system at such low pressures. In addition, the ability to operate at low pressures has allowed the low energy electrons tracks to be clearly resolved. Although this has been demonstrated using charge readouts (e.g., a pixellated readout) for 5.9 keV recoils [4, 5] and optically for 15-22 keV recoils [6, 7], to our knowledge this is the first time it has been done using optical imaging for ^{55}Fe energies.

The detector used for the measurements was a low pressure TPC (time projection chamber) operating in 99.999% CF_4 with GEM (gas electron multiplier) and thick GEM (THGEM) amplification, and a CCD-based optical readout. GEMs are a micro-pattern amplification device invented by Sauli at the European Organization for Nuclear Research (CERN) [8]; further information on the operation of GEMs with CCD readout can be found in Refs. [1, 9, 10, 11, 12, 13]. THGEMs are very similar to GEMs but with dimensions (thickness, hole size, and pitch) that are typically about one order of magnitude larger. Exceptionally high gas gains have been achieved in both types of amplification devices, but the THGEMs have been shown to excel at the very low pressures of interest here [14].

2. Detector Setup

A schematic of the detector setup is shown in Figure 1. At each pressure, the choice of amplification device between single GEM/THGEM or multiple GEMs/THGEMs was made to maximize stability, gas gain, and spatial resolution. For the 100 Torr measurements, the detector used a cascade of three standard copper GEMs separated by 2 mm (Figure 1). The GEMs were manufactured at CERN using a 50 μm thick, 7 × 7 cm^2 sheet of kapton. The sheet was copper-clad on both surfaces (~5 μm thick) and chemically etched with a hexagonal array of bi-conical holes of diameter of 50/70 μm (inner/outer), at a pitch of 140 μm. For a thorough review of GEMs, see Ref. [15]. A 7 × 7 cm^2 cathode was located 1 cm below the GEM stack, defining the detection/drift volume. The cathode was constructed from a ~ 360 μm thick copper mesh with ~500 μm pitch. Finally, a 1 mm pitch anode wire grid plane made from 20 μm thick gold plated tungsten wires was situated 3 mm above the top-most GEM (GEM 3), forming the induction gap (further details of this detector can be found in Ref. [13]).

At pressures below 100 Torr we replaced the triple-GEM cascade with THGEMs, which are better suited for high gain operation at low pressures [14]. Even going from 100 Torr to 75 Torr, for example, the maximum stable gas gain in the triple-GEM detector was no longer sufficient to image ^{55}Fe tracks.[1] All THGEMs used in our studies were fabricated at CERN using a 0.4 mm thick PCB with ~0.3 mm holes mechanically drilled in a hexagonal pattern with a pitch of ~0.5 mm. To

*Corresponding author

[1] In addition, due to the lower ionization (scintillation) density of the longer tracks at lower pressures, it is not sufficient to simply maintain gas gain.

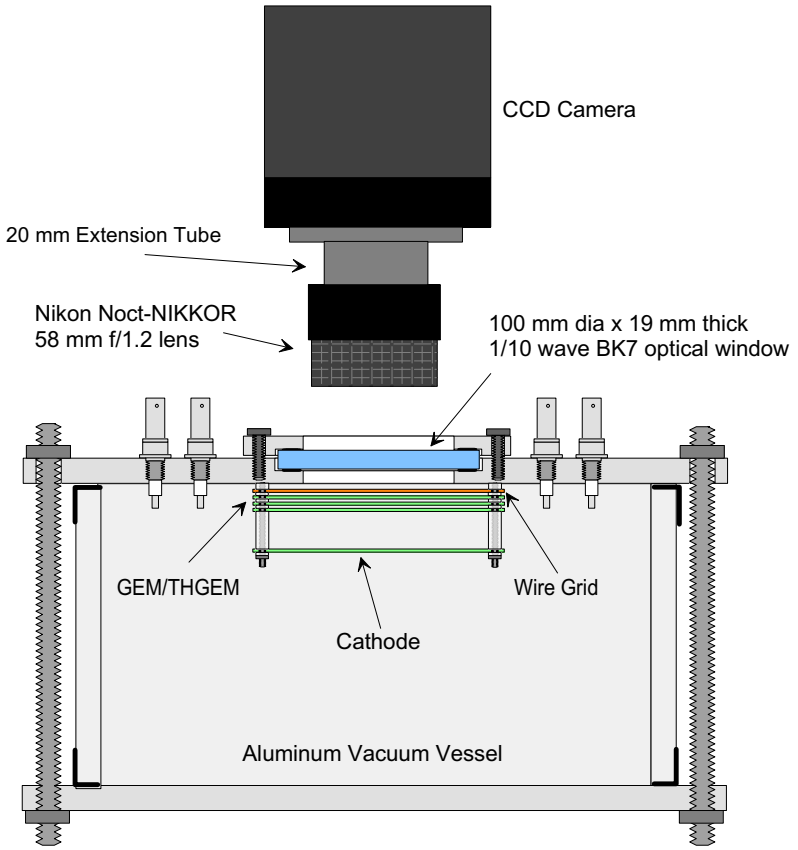

(a) Detector Vessel

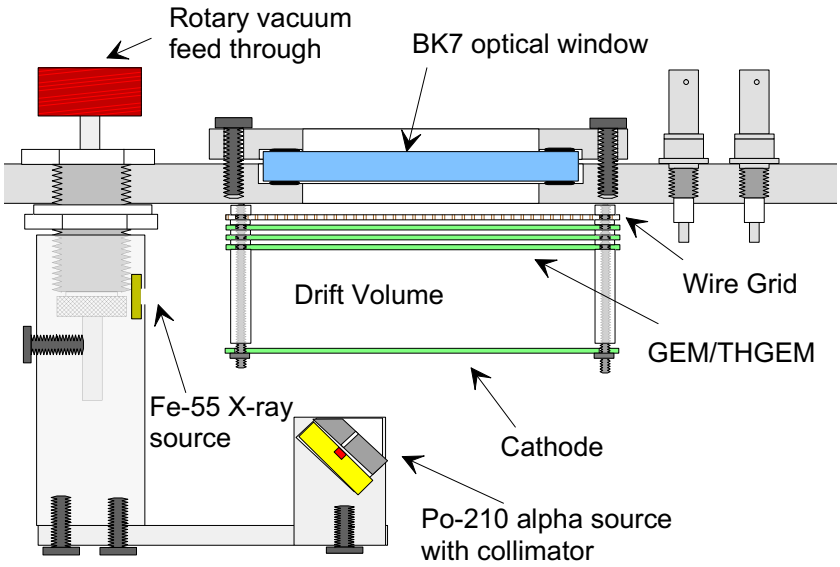

(b) Detection Volume

Figure 1: (a) A simplified drawing of the CCD detector showing the aluminum vacuum vessel and CCD camera setup, excluding the rotary feedthrough, camera mount, and calibration sources for clarity. The light blocking box is also excluded to show the lens and extension tube. (b) A close up view of the detection volume, showing the locations of the calibration sources, cathode, wire grid, and GEMs/THGEMs.

eliminate burring from the drilling process, an annular region of thickness 0.05 mm was chemically etched around each hole.

In our 50 Torr measurements a single THGEM with an active region of 3×3 cm^2 was used. To better accommodate the longer tracks at these low pressures, the drift gap was increased from 1 cm to 2 cm. In addition, the separation from the amplification device and the wire grid was increased from 3 mm to ~7 mm, which provided better stability at the lower pressures.

For the 35 Torr measurements a double-THGEM, with a 9.5×9.5 cm^2 active area[2], was required to achieve the necessary gas gain. The drift gap, transfer gap between the THGEMs, and induction gap between the THGEM and wire grid were 2 cm, 4 mm, and 9.5 mm, respectively. In addition, the wire grid size was increased to match the THGEM area by laying copper tape around the perimeter of the wire frame.

For all measurements, the detector was housed inside a ~10 liter cylindrical aluminum vacuum vessel. Calibration was done using internally mounted ^{55}Fe (5.9 keV X-rays) and ^{210}Po (5.3 MeV alphas) sources, which could be individually turned on or off using a rotary feed-through (Figure 1b). Prior to powering up the GEMs/THGEMs, the vacuum vessel was pumped out to < 0.1 Torr for at least one day before back-filling with pure (99.999%) carbon tetrafluoride (CF_4) gas. A 4-inch diameter BK-7 glass window was positioned above the wire grid to allow scintillation light from the final amplification stage to be captured and imaged by the lens and CCD camera. BK-7 is a material with a relatively high transmittance for the optical component of the CF_4 scintillation, which peaks around 620 nm [16, 17], and is lower cost compared to quartz.

The optical system consisted of a fast 58 mm f/1.2 Nikon Noct-NIKKOR lens mated to a back-illuminated Finger Lakes Instrumentation (FLI) CCD camera (MicroLine ML4710-1-MB) through a 20 mm extension tube for close-focus imaging. The whole setup was mounted on top of the vacuum vessel (Figure 1a) in a light tight box. The camera contained an E2V 18.8 mm diagonal sensor with a 1024×1024 pixel array (CCD47-10-1-353), consisting of 13×13 μm^2 pixels. The mid-band coated CCD sensor had a peak quantum efficiency of 96% at 560 nm and could be cooled down to a stable operating temperature of −38°C using the built-in Peltier cooler. Two readout speeds were available, 700 kHz and 2 MHz, with 16-bit digitization and a maximum 16×16 on-chip pixel binning. At the lowest operating temperature and slowest readout mode, the read-out noise was ~10 e$^-$ rms and the dark current was ~0.03 e^-/pix/sec with 1×1 on-chip pixel binning. At our focusing distance, the CCD-lens system imaged a ~3×3 cm^2 physical region of the GEM/THGEM surface. The known pitch of the holes on this surface was used to calibrate the length-scale of the images.

3. Detector Calibrations

3.1. GEM/THGEM Gain

The gas gain was determined using an ORTEC 448 research pulse generator and an ORTEC 142IH charge sensitive preamplifier, which read out the charge signal from the last GEM/THGEM surface. The pulse generator output was connected to the test input of the preamplifier via a built-in 1 pF capacitor for calibration purposes. This allowed the preamplifier gain (fC/V) to be determined. The 5.9 keV ^{55}Fe X-ray calibration source was then used to determine the effective gas gain from the output voltage signal of the preamplifier. The conversion of the X-ray created 172 electron-ion pairs on average, which was calculated from the W-value (the average energy per ionization) of 34.2 eV for CF_4 [18].

For each pressure the maximum stable gain was determined iteratively by raising the GEM/THGEM voltages and testing for stability. The latter was done by firing a highly ionizing source (^{210}Po alpha source) into the detection volume. If no sparks occurred over several hours, then the voltage setting was deemed stable and the procedure repeated until the maximum stable gain was found.

At a pressure of 100 Torr, a maximum stable effective gain of ~ 1×10^5 was achieved with GEM 1 = 279 V, GEM 2 = 334 V, and GEM 3 = 380 V, and a drift field of 400 V/cm. At these GEM voltages the transfer fields were 1.40 kV/cm and 1.67 kV/cm between GEMs 1 and 2, and 2 and 3, respectively, and the induction field was 260 V/cm between GEM 3 and the grid. A higher effective gas gain of ~ 2×10^5 was achieved with GEMs 1 and 2 = 290 V and GEM 3 = 450 V, where the drift, transfer, and induction fields were 400 V/cm, 1.45 kV/cm, and 360 V/cm, respectively. This setting, however, was not entirely stable under alpha irradiation, which initiated a spark about once per hour. Nevertheless, we were able to acquire ^{55}Fe images and an energy spectrum without any sparks at this setting.

For the 50 Torr measurements, the THGEM was powered to a voltage of 830 V and the drift field was set to 200 V/cm (same E/p as in the 100 Torr measurements). The induction field was 824 V/cm with the wire grid set to a lower voltage than the top THGEM surface so that all electrons produced in the avalanche were collected by this electrode. The electrical stability at this voltage setting was similar to the highest gain setting at 100 Torr in that both were moderately but not completely stable. For this measurement we estimate the gain to be ~ 1.5×10^5.

Finally, in the 35 Torr measurements, the THGEM voltage biases were THGEM 1 = 573 V and THGEM 2 = 470 V, where THGEM 1 is the one facing the cathode and THGEM 2 is nearest to the wire grid. The drift, transfer, and induction fields were 200 V/cm, 718 V/cm, and 495 V/cm, respectively. Here we estimate the gas gain, which was stable, to be ~1.6×10^5.

3.2. CCD Calibration

The CCD images (or frames) were calibrated using a set of co-averaged flat-field and dark frames. Both were taken with the same 5 second exposure time as the data images. Dark frames, taken with the camera shutter closed, were used to correct for the variable accumulation rate of dark current across the pixels in the CCD sensor. Flat-field frames, used to correct for vignetting and pixel to pixel variation in light sensitivity, were acquired by taking exposures of a uniformly illuminated screen. For each type of calibration frame, a set was acquired and co-averaged together to create a master calibration frame.

[2] Two 3×3 cm^2 THGEMs were not available.

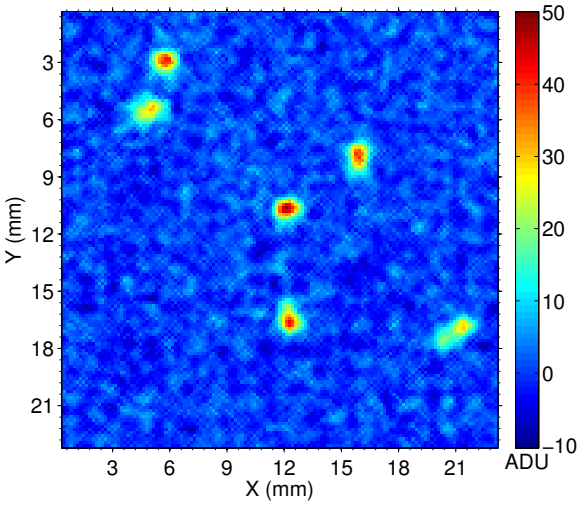

(a) ^{55}Fe tracks in 100 Torr CF_4

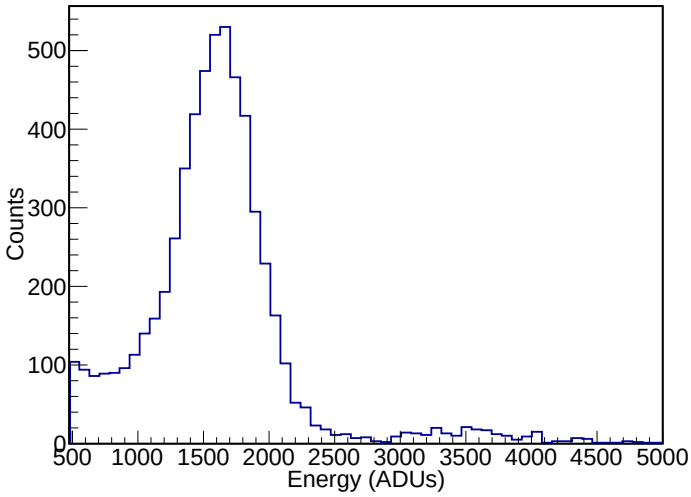

(b) ^{55}Fe energy spectrum at 100 Torr CF_4

Figure 2: (a) An image of ^{55}Fe tracks acquired at 6×6 on-chip binning (pixel scale of 165 μm/pix) in 100 Torr CF_4 with an averaging filter of block size 5×5 applied to the image to enhance signal-to-noise. The image is captured at the maximum stable gas gain of $\sim 10^5$ and has a pixel scale of 165 μm/pix. (b) An energy spectrum of ^{55}Fe obtained optically from CCD imaging of electronic recoil tracks at 6×6 on-chip binning and the maximum stable gain. The data is a combination of the start and end data sets in the day eight run (see Figure 8). The smaller secondary feature to the right of the primary peak is the result of event pile-up.

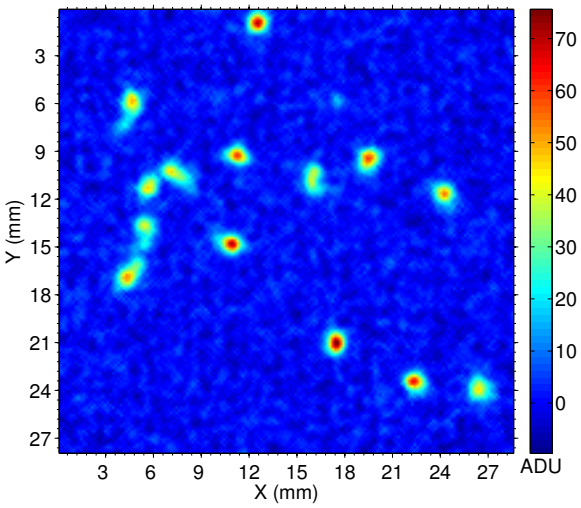

(a) ^{55}Fe tracks in 100 Torr CF_4

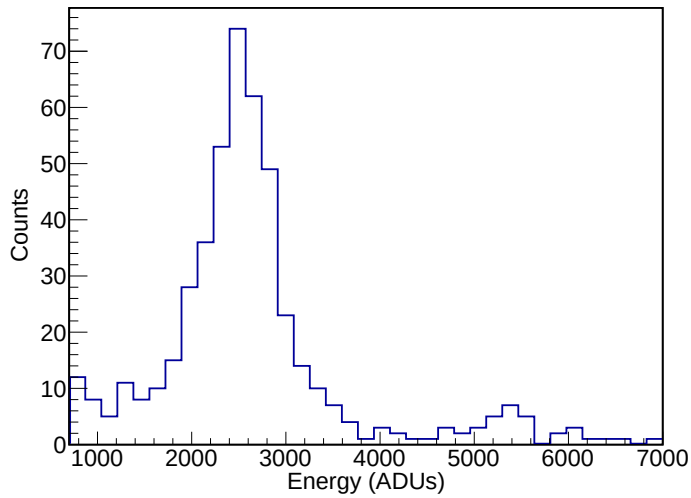

(b) ^{55}Fe energy spectrum at 100 Torr CF_4

Figure 3: (a) An image of ^{55}Fe tracks acquired at 6×6 on-chip binning in 100 Torr CF_4 with an averaging filter of block size 5×5 applied to the image to enhance signal-to-noise. The image is captured at the maximum gas gain of $\sim 2 \times 10^5$ and shows that even in 100 Torr, ^{55}Fe tracks are resolved. (b) An ^{55}Fe energy spectrum obtained optically from CCD imaging of electronic recoil tracks at 6×6 on-chip binning and maximum gain of $\sim 2 \times 10^5$. The smaller secondary feature to the right of the primary peak is due to event pile-up.

For accuracy, the averaging required rejecting pixels in individual frames that suffered direct hits from cosmic rays or radioactivity. This was done using an algorithm that compared the value of the same pixel across the set of frames, excluding those above three sigmas of the initial average of the pixels. The average was re-computed and the process iterated until there was a convergence in the average value of the pixels. Finally, the data image was calibrated by subtracting the master dark frame and dividing the resulting frame by the normalized, master flat-field frame.

4. Results

4.1. 100 Torr

A sample image containing ^{55}Fe tracks taken at the maximum stable gain setting in 100 Torr CF_4 is shown in Figure 2a. On chip binning of 6×6 was used for this image, resulting in each binned pixel imaging 165 μm in real space. The signal is well above the noise in the CCD image and individual tracks are resolved. With this level of signal-to-noise and resolution one could easily characterize the spatial uniformity of the gas gain across the GEMs.

The corresponding optically derived energy spectrum, using images of these tracks, is shown in Figure 2b in units of ADUs[3]. The peak value in the spectrum is obtained from a fit which comprises of a single Gaussian signal component and a constant plus exponential for the background components. The range of the fit is set so as to exclude the secondary peak seen at ~3500 ADU, which is due to pile-up events. The fit has a reduced χ^2 (χ^2/ndf) = 0.66, a peak value of $\mu_{100\text{Torr}} = 1621 \pm 5$, and $\sigma_{100\text{Torr}} = 264 \pm 5$. The FWHM energy resolution is 38% and we obtain an energy conversion factor of 275 ADUs/keV.

In Figures 3a and 3b, a sample image of ^{55}Fe tracks imaged at 6×6 binning and a higher gain of ~$2{\times}10^5$ in 100 Torr CF_4 is shown along with the corresponding energy spectrum. The same procedure for fitting the spectrum as described above gives a peak value of 2505 ± 25, σ of 324 ± 29, and energy conversion factor of 425 ADUs/keV. Interestingly, the FWHM energy resolution is 30%, significantly better than that of the moderate gain 100 Torr data at the same image binning.

For the 16×16 high gain data, a sample image of ^{55}Fe tracks and the corresponding energy spectrum are shown in Figures 4a and 4b. A fit of the spectrum gives a peak value of 2615 ± 14, σ of 331 ± 16, and energy conversion factor of 443 ADUs/keV. The 4% difference in peak value between the 6×6 and 16×16 data could be the result of a reduced efficiency for finding the entire track due to a slightly lower signal to noise in the lower binned data. Alternatively, the difference could simply be due to drift in the gas gain over time between acquisition of the two data sets. Both high gain data sets, however, have the same FWHM energy resolution of 30%.

4.2. 25, 35 & 50 Torr

In Figure 5, two sample images of ^{55}Fe tracks taken at a pressure of 50 Torr in CF_4 are shown. As expected, the tracks are longer and much better resolved than those in the 100 Torr data and, additionally, differences in ionization density are also clearly visible. The corresponding energy spectrum is not shown because not enough images were taken at this pressure due to onset of electrical instability, which is not surprising given the low operating pressure and high gas gain. Nevertheless, as these images unambiguously show, CCD-based TPCs with sufficiently high signal-to-noise and imaging resolution can *resolve* electron recoils with energies as low as 5.9 keV.

For the 35 Torr data, a sample image containing ^{55}Fe tracks is shown in Figure 6a. As in the 50 Torr data the tracks are clearly resolved but the resolution is poorer due to the presence of a second THGEM and the transfer region within the double THGEM amplification structure. The energy spectrum obtained from a series of these images is shown in Figure 6b. A fit of the spectrum to a single Gaussian signal component and a background component which consists of uniform and exponential components gives a reduced χ^2 (χ^2/ndf) = 0.80. The fitted peak value is $\mu_{35\text{Torr}} = 2327 \pm 18$ and $\sigma_{35\text{Torr}} = 400 \pm 28$. This gives a FWHM energy resolution of 40% which is similar to, within errors, the energy resolution obtained from the moderate gain 100 Torr data.

Finally, in Figure 7, we present sample images of ^{55}Fe tracks acquired at a pressure of 25 Torr pure CF_4. However, there is insufficient data for an energy spectrum because electrical instabilities (discharges) prevented a long data run. But with additional fine tuning of THGEM voltages and detector setup, it is conceivable that stable operation at this pressure with sufficient gas gain for imaging individual ^{55}Fe tracks could be achievable.

4.3. Light Yield and Contaminants

Two effects on the light yield in 100 Torr CF_4 were observed in our ^{55}Fe calibration data. The first was due to contamination from out-gassing, and the second was an indication of light quenching at high gas gains. We discuss these here.

^{55}Fe calibrations were required over 8 days for a different application[4], providing us data to study the effects of possible gas contaminants on the light yield. Before the start of the 8 day data run, the detector vessel was sealed and pumped out to <0.1 Torr overnight. Subsequently, each day of data taking started by back-filling the detector vessel to 100 Torr with 99.999% pure CF_4, powering up the detector and acquiring ~70 minutes of ^{55}Fe data. This was followed by ~14 hours of neutron data and a second ~70 minute ^{55}Fe exposure at the end of the day, after which the detector was powered down and the vessel pumped out for ~3 hours. This procedure was repeated for each day of data taking. The GEMs were powered up to the same voltages each day, with the values given in Section 3.1 for the moderate,

[3] Analog to Digital Units, with 1 ADU equal to ~1.3 e^- produced in our CCD sensor.

[4] These were acquired for calibration of neutron exposures of the detector for directional studies.

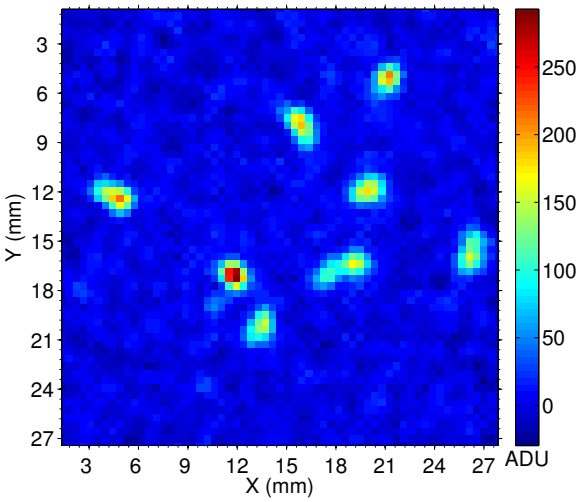

(a) ^{55}Fe tracks in 100 Torr CF_4

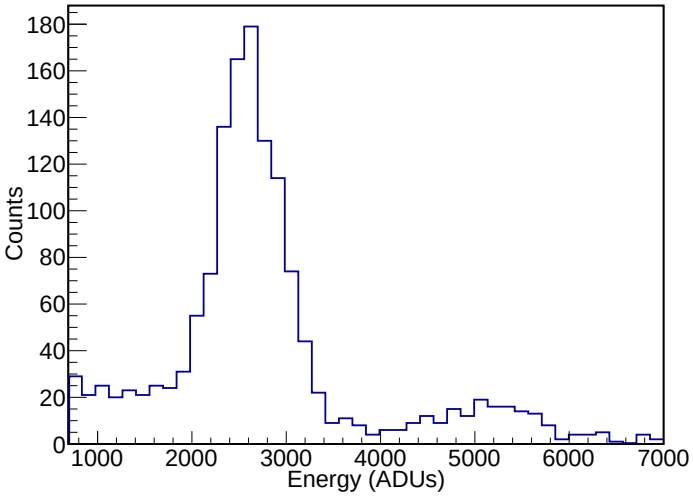

(b) ^{55}Fe energy spectrum at 100 Torr CF_4

Figure 4: (a) An image of ^{55}Fe tracks acquired at 16×16 on-chip binning (pixel scale of 440 µm/pix) in 100 Torr CF_4 with an averaging filter of block size 3×3 applied to the image to enhance signal-to-noise. The image is captured at the maximum gas gain of $\sim 2 \times 10^5$ and shows that even in 100 Torr, ^{55}Fe tracks are resolved. (b) An ^{55}Fe energy spectrum obtained optically from CCD imaging of electronic recoil tracks at 16×16 on-chip binning and maximum gain of $\sim 2 \times 10^5$. The smaller secondary feature to the right of the primary peak is due to event pile-up.

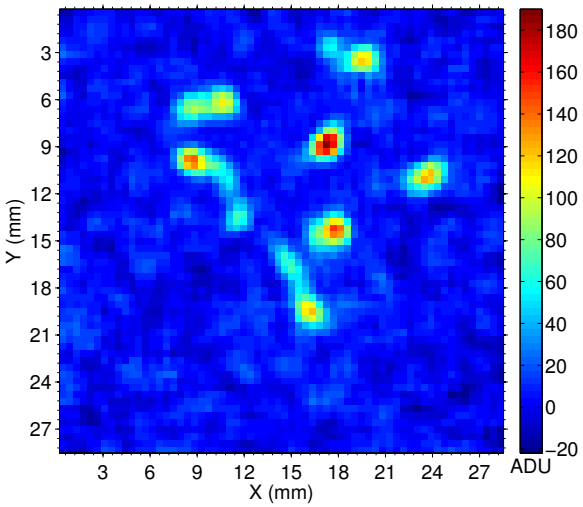

(a) ^{55}Fe tracks in 50 Torr CF_4

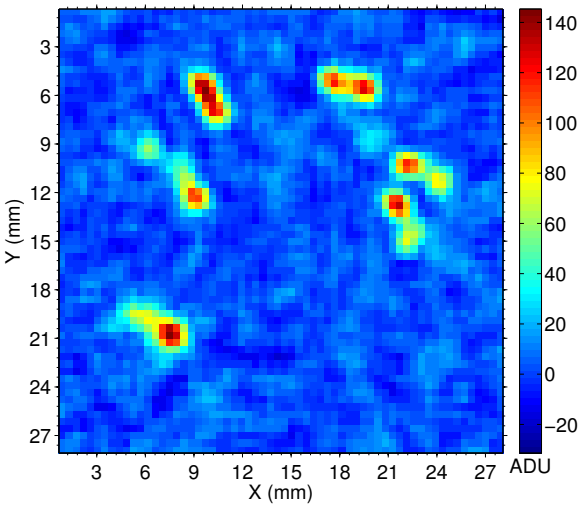

(b) ^{55}Fe tracks in 50 Torr CF_4

Figure 5: (a)-(b) Images of 5.9 keV ^{55}Fe electronic recoil tracks in 50 Torr CF_4 at 16×16 on-chip binning. An averaging filter with a 3×3 block size has been applied to the image to improve signal-to-noise without significantly degrading resolution. At this pressure, the tracks are well resolved and fluctuations in energy loss and range straggling are also clearly observable.

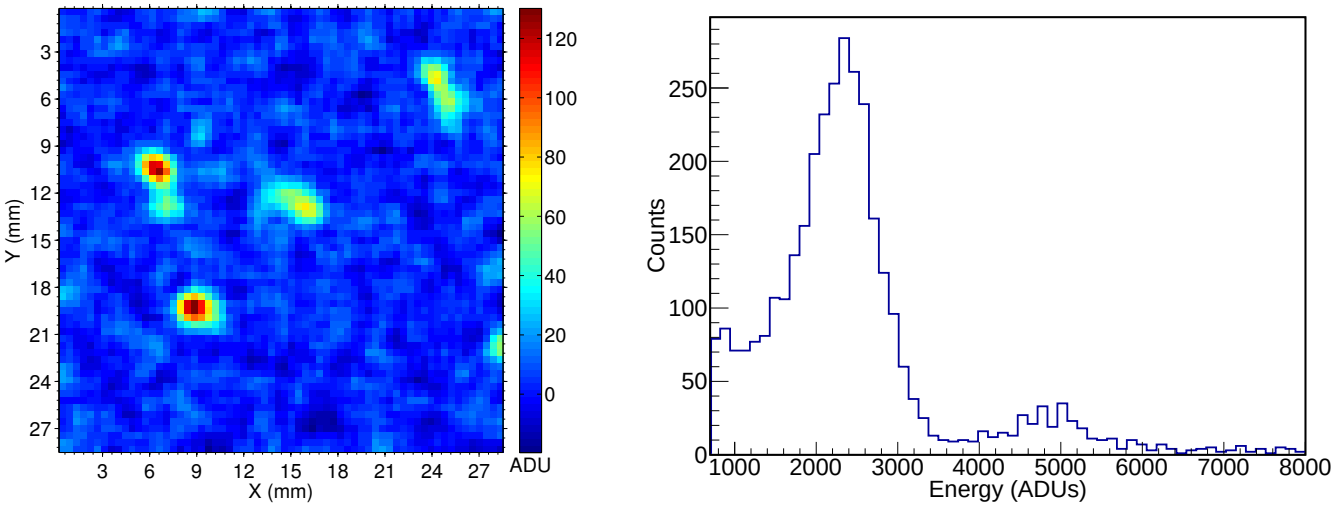

(a) ^{55}Fe tracks in 35 Torr CF_4

(b) ^{55}Fe energy spectrum at 35 Torr CF_4

Figure 6: (a) An image of ^{55}Fe tracks in 35 Torr CF_4 with an averaging filter applied to enhance signal to noise. The tracks are clearly resolvable as extended objects rather than diffused points at this pressure. (b) An energy spectrum obtained from CCD imaged ^{55}Fe electronic recoil tracks in 35 Torr at 16×16 on-chip binning and maximum stable gain. The smaller secondary feature on the right of the primary peak is due to event pile-up.

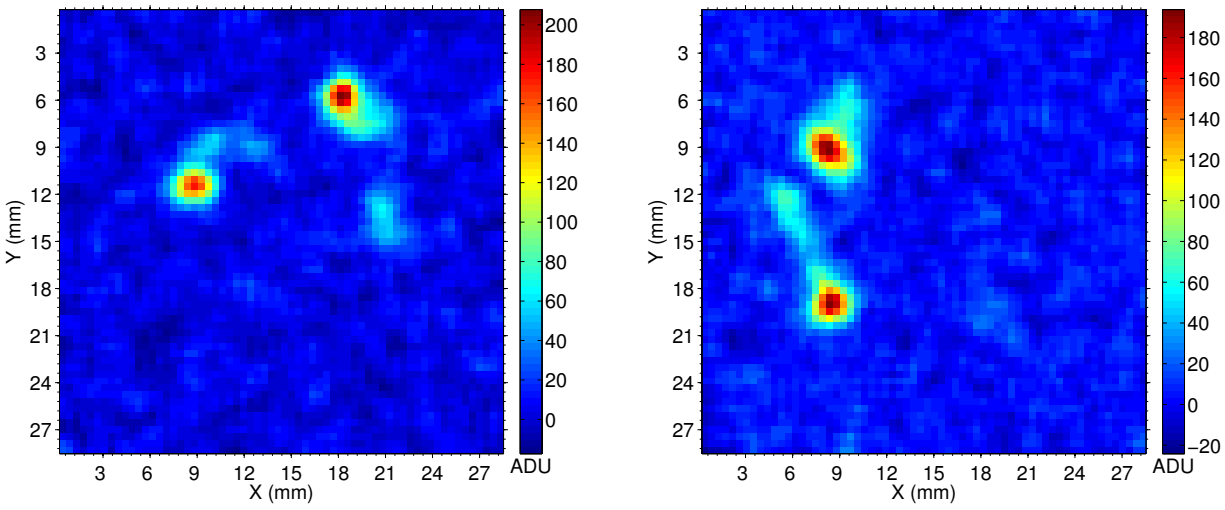

(a) ^{55}Fe tracks in 25 Torr CF_4

(b) ^{55}Fe energy spectrum at 25 Torr CF_4

Figure 7: (a)-(b) Sample images of ^{55}Fe tracks in 25 Torr CF_4 using two THGEMs and 16×16 CCD on-chip binning. A 5×5 averaging filter has been applied to enhance signal to noise. The tracks are resolvable at this pressure and gas gain.

stable gas gain of $\sim 1\times10^5$. The electronic ^{55}Fe spectrum was used to monitor the gas gain, which remained constant within 10% over the 8 days. The optical ^{55}Fe data over this period, however, showed an increase in the light yield, which is highly sensitive to gas purity. With the detector kept sealed over the 8 days, out-gassing would be the main source of contamination with the expectation that its rate would decrease over time.

The results of the data runs are plotted in Figure 8, which shows the fitted peak value of the optical ^{55}Fe spectrum at the start and end of each of the 8 days of data acquisition. The large difference in the start and end spectrum peak values for data run 1 is most likely the result of insufficient time given between GEM power up and data taking; we found that the GEMs required about 1-2 hours after being brought up to voltage before stable operation ensued.

With the exception of run 1, the start and end spectrum peak values are always within 4% of each other, which suggests that that any compositional change of the gas does not affect the light output significantly over a single day. The data, however, shows a clear rise in the spectrum peak value over the 8 days. Between run 2 and run 8 the light output increased by 21% in the end series, and by 19% in the start series. The light yield in the end series is monotonically increasing whereas that in the start series has scatter due to variability in the time between GEM power up and data taking. Nevertheless, the steady increase in light yield over the 8 days is consistent with improved gas purity due to a decrease in the out-gassing rate, which can have a long half-life in sealed vessels that have not been baked out.

The second effect, possibly due to light quenching, was the change in the ratio of the optical ^{55}Fe spectrum peak and the corresponding effective gas gain for the two gain settings, $\sim 1\times10^5$ and $\sim 2\times10^5$. In the lower gain data, this ratio was ~ 0.016, and in the high gain data it was ~ 0.013. This ratio, which can be thought of as an effective photon yield (photons per secondary electron), is lower by $\sim$19% at the higher gas gain. Unfortunately, the low and high gain measurements were taken months apart so it is difficult to definitively attribute the lower photon yield to quenching. We nevertheless describe the various possibilities as some of them have important implications for applications such as directional dark matter searches.

The first possibility is that it could be a charge density effect, where the photon yield decreases (is quenched) as the charge density increases at high gas gains. Of course, the emission spectrum from CF_4 could also be affected at high charge densities, lowering the number of photons produced in the wavelength range of sensitivity for our CCD camera and lens. Another possibility is that there were more contaminants due to out-gassing in the high gain measurements, which could also explain the lower light yield.

Lower light yields resulting from contamination due to out-gassing could be dealt with with a long pump down and/or continuous filtering of the gas in a circulation system. However, quenching due to high charge density arising from either high gas gains and/or high primary ionization densities has important consequences for applications where measuring the charge density along a recoil track is required. An example is directional dark matter detection in which the sense (vector direction) of the ionization track is determined by measuring the asymmetry in the charge deposition along the track. If quenching plays a significant role in the low pressure regime where directional dark matter experiments operate, it could limit how well the directional signature can be measured in gas based TPCs operated at high gas gains.

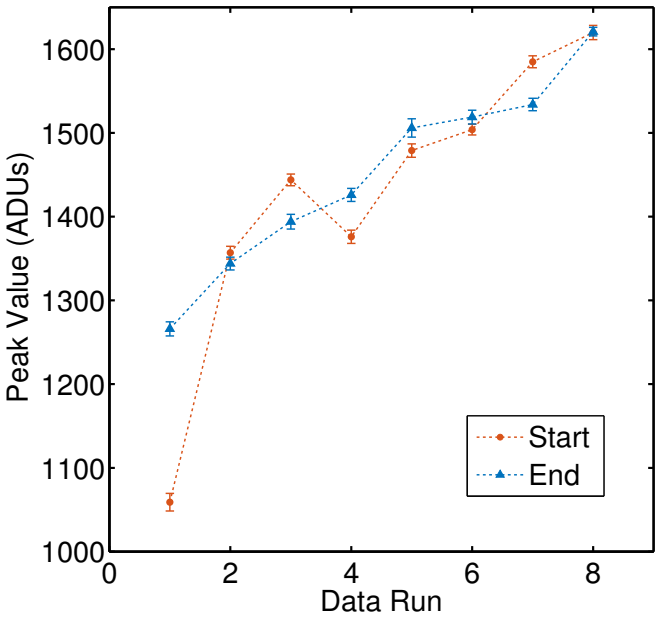

Figure 8: The fitted peak value of the ^{55}Fe energy spectrum at the start and end of the day over eight days of data taking. With the exception of the first data run, the start and end peak values are within 4%. The large change ($\sim$ 20%) seen between the start and end in the first data set is likely due to insufficient time for the GEMs to charge up and stabilize. The raising peak value with run number is likely the result of a reduction in concentration of contaminants with the additional pump down in-between runs.

5. Conclusion

We have shown that a GEM and THGEM based detector can be operated in low pressure CF_4 (25-100 Torr) with gains exceeding 2×10^5. This allowed individual ^{55}Fe tracks to be imaged by a low noise CCD camera and for an optically measured spectrum to be obtained. We found that it is important to pump down the detector for an extended period of time to reduce contaminants in the gas that can suppress light output. We also noted a decrease in light yield at higher gas gains, which could be due to light quenching at high charge densities. If confirmed, this could affect directional dark matter experiments that rely on the asymmetry in charge density to determine the recoil direction of a track. Finally, we showed that electronic recoils as low as 5.9 keV in energy can be optically resolved. This is important for rare event searches such as direct dark matter detection experiments that rely on differences in stopping power to discriminate between different types of recoils.

Acknowledgements

This material is based upon work supported by the NSF under Grant Nos. 0548208, 1103420, and 1407773.

References

[1] F. A. F. Fraga, et al., Nucl. Instr. and Meth. Phys. Res. A 513 (2003) 379-387.
[2] H. Sakurai, et al., Nucl. Instr. and Meth. Phys. Res. A 513 (2003) 282-286.
[3] F. Tokanai, et al., Nucl. Instrum. and Meth. Phys. Res. A 571 (2007) 289-293.
[4] R. Bellazzini, et al., Nucl. Instr. and Meth. Phys. Res. A 510 (2003) 176-184.
[5] J. K. Black, P. Deines-Jones, S. E. Ready, R. A. Street, Nucl. Instr. and Meth. Phys. Res. A 513 (2003) 639-643.
[6] H. Sakurai, et al., Nucl. Instr. and Meth. Phys. Res. A 505 (2003) 219-222.
[7] H. Sakurai, et al., Nucl. Instr. and Meth. Phys. Res. A 525 (2004) 6-11.
[8] F. Sauli, Nucl. Instr. and Meth. Phys. Res. A 386 (1997) 531-534.
[9] F. A. F. Fraga, et al., Nucl. Instr. and Meth. Phys. Res. A 442 (2000) 417-422.
[10] F. A. F. Fraga, et al., Nucl. Instr. and Meth. Phys. Res. A 471 (2001) 125-130.
[11] F. A. F. Fraga, et al., Nucl. Instr. and Meth. Phys. Res. A 478 (2002) 357-361.
[12] L. M. S. Margato, et al., Nucl. Instr. and Meth. Phys. Res. A 535 (2004) 231-235.
[13] N. S. Phan, R. J. Lauer, E. R. Lee, D. Loomba, J. A. J. Matthews, E. H. Miller, Astropart. Phys. 84 (2016) 82-96.
[14] C. K. Shalem, R. Chechik, A. Breskin, K. Michaeli, N. Ben-Haim, Nucl. Instr. and Meth. Phys. Res. A 558 (2006) 468-474.
[15] A. F. Buzulutskov, Instr. Exp. Tech., 2007, Vol. 50, No. 3, pp. 287.
[16] A. Morozov, et al., Nucl. Instr. Meth. Phys. Res. B 268 (2010) 1456-1459.
[17] A. Kaboth, et al., Nucl. Instr. and Meth. Phys. Res. A 592 (2008) 63-72.
[18] G. F. Reinking, L. G. Christophorou, S. R. Hunter, J. Appl. Phys. 60, 499 (1986).